JOURNAL OF MATERIALS PROCESSING TECHNOLOGY 206 (2008) 425–430

journal homepage: www.elsevier.com/locate/jmatprotec

Fabrication and characterization of eutectic gold–silicon (Au–Si) nanowires

Jin-Shyong Lin[a], *Chien-Chon Chen*[b], *Eric Wei-Guang Diau*[b,*], *Tzeng-Feng Liu*[a]

[a] *Department of Material Science and Engineering, National Chiao Tung University, Hsinchu 30010, Taiwan*
[b] *Department of Applied Chemistry and Institute of Molecular Science, National Chiao Tung University, Hsinchu 30010, Taiwan*

ARTICLE INFO

Article history:
Received 13 April 2007
Received in revised form
5 November 2007
Accepted 15 December 2007

Keywords:
AAO
Au–Si alloy
Die-casting
Eutectic nanowire
Vacuum smelting

ABSTRACT

Hypoeutectic, eutectic and hypereutectic gold–silicon (Au–Si) alloys were synthesized using vacuum smelting. When Au and Si were smelted in a vacuum chamber near 1100 °C, $Si_{(g)}$, $Si_{2(g)}$, $Si_{3(g)}$, $SiO_{2(g)}$, $Au_{(g)}$, $SiO_{2(s)}$ and $Au_2O_{3(s)}$ were formed rapidly; the quantities of Au and Si lost were estimated from thermodynamic formulas. The nano- and microstructures of the Au–Si eutectic compound were characterized with a SEM and a TEM, which showed a discontinuous phase of Si dispersed and mounted within a matrix phase of Au. Cracks that formed about the Au–Si interface made the Au–Si eutectic brittle. From an Au–Si alloy of superior quality as a bulk material, eutectic nanowires of average diameter 60 nm were fabricated after the alloy was melted and injected into an anodic aluminum-oxide (AAO) template.

1. Introduction

Gold is a conductive noble metal, and silicon is a base material for the semiconductor industry. Gold is commonly used in semiconductor products. For example, an Au–Si eutectic alloy is used for microchip packing and interconnection in micro-electro-mechanical systems (MEMS). As an Au–Si eutectic has a useful field-emission property, it serves for panels or displays; for example, a 70-nm Au–Si eutectic tip has an initiating field only 10 V μm^{-1} (Wan et al., 2004). Furthermore, when an Au–Si eutectic is set on a 10-μm tip, a large field current 300 μA is obtainable on the tip (Zhirnov et al., 1996). Although such an Au–Si alloy has excellent electronic characteristics, the mechanical properties of such an Au–Si alloy are generally detrimental to product quality. According to Komatsu and Kiritani (2003), an Au–Si eutectic becomes brittle upon subjection to the cold-rolling process. Gold is a ductile material, but a small proportion of brittle silicon in gold makes the alloy become brittle.

According to the Au–Si binary phase diagram (Massalski, 1987) shown in Fig. 1, the melting points of Au and Si are 1064 °C and 1414 °C, respectively, whereas the eutectic point has a melting point only 363 °C. No compound formation of any composition occurs in an Au–Si alloy, but three alloy phases – hypoeutectic, eutectic and hypereutectic – appear in the Au–Si diagram. When the temperature is greater than that of the liquid line, mixed Au and Si in a liquid phase appear; hypoeutectic and hypereutectic phases appear when the temperature decreases along hypoeutectic and hypereutectic lines.

The fabrication of nanowires by non-lithographic methods such as ion deposition has been reported (Komatsu and Kiritani, 2003; Massalski, 1987; Wang et al., 2001; Zhang et al., 2000; Nielsch et al., 2001). Problems are associated with ion

* *Corresponding author*. Fax: +886 3 572 3764.
E-mail addresses: chentexas@gmail.com (C.-C. Chen), diau@mail.nctu.edu.tw (E.W.-G. Diau).
0924-0136/$ – see front matter © 2008 Elsevier B.V. All rights reserved.
doi:10.1016/j.jmatprotec.2007.12.069

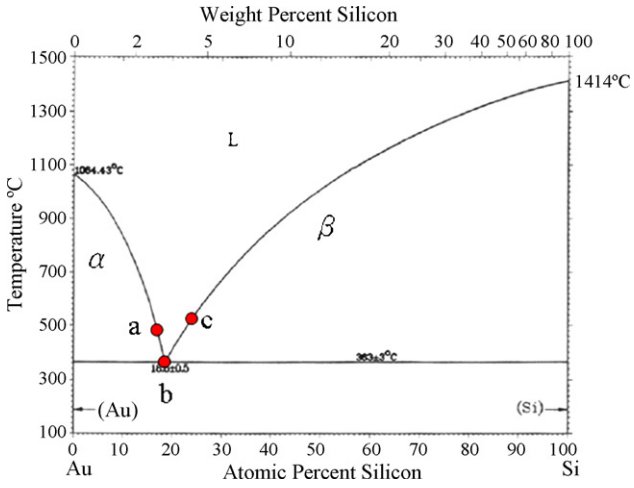

Fig. 1 – Au–Si phase diagram: hypoeutectic composition of point a (2.3 mass% Si–Au), eutectic composition of point b (2.8 mass% Si–Au), and hypereutectic composition of point c (4.0 mass% Si–Au).

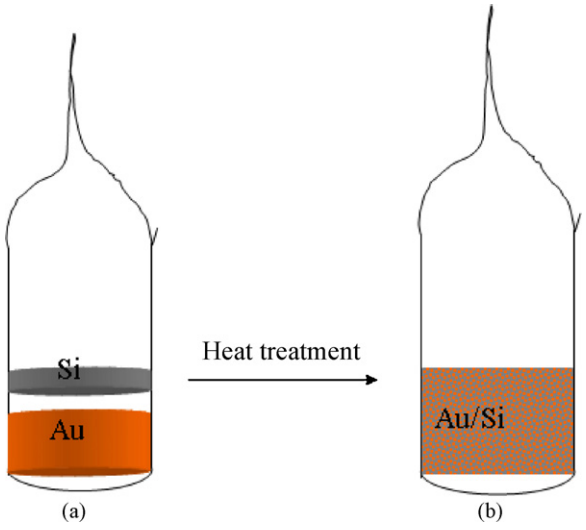

Fig. 2 – Schematic diagram of Au–Si alloys made with vacuum smelting: (a) ratio (mass%) of Au and Si in the vacuum tube and (b) after heating, Au–Si alloys formed in the tube.

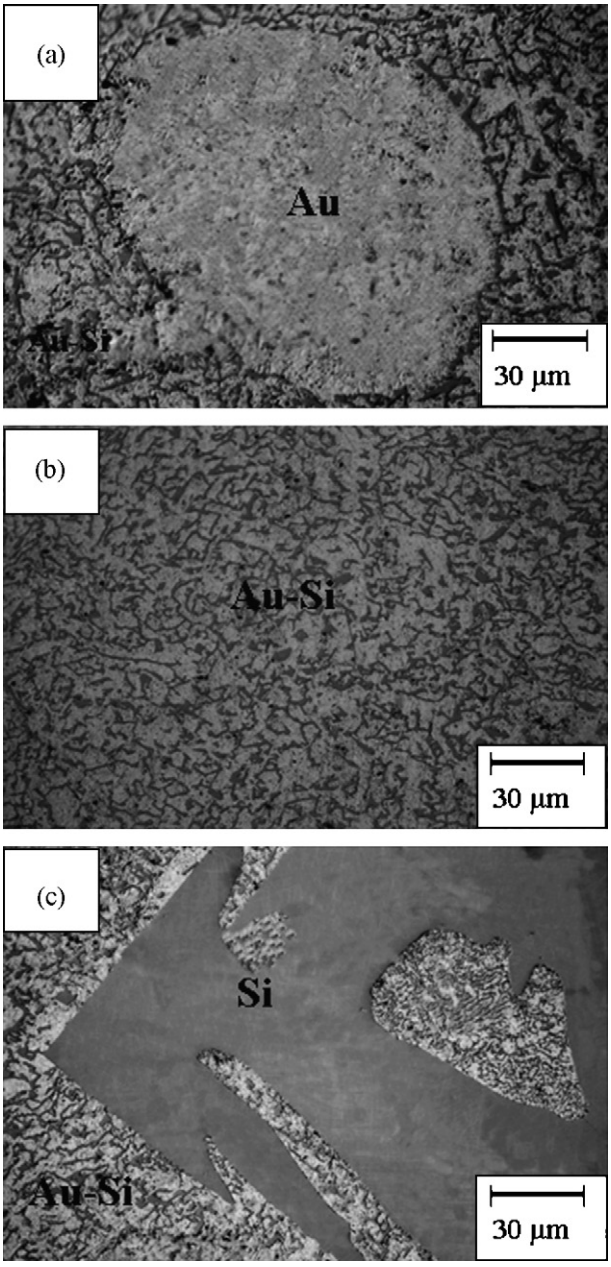

Fig. 3 – OM images of Au–Si alloys: (a) Si–Au of hypoeutectic (2.3 mass%), (b) Si–Au of eutectic (2.8 mass%), and (c) Si–Au of hypereutectic (4.0 mass%).

Table 1 – Thermodynamic equilibrium reactions in the Au–Si–O system

Reaction	Equations	log *K*
$Si_{(s)} \rightarrow Si_{(g)}$	$\log P_{Si_{(g)}} = \log K$	7.694 – (23447.16/T)
$2Si_{(s)} \rightarrow Si_{2(g)}$	$\log P_{Si_{2(g)}} = \log K$	3.505 – (26942.52/T)
$3Si_{(s)} \rightarrow Si_{3(g)}$	$\log P_{Si_{3(g)}} = \log K$	10.465 – (32920.81/T)
$Si_{(s)} + O_{2(g)} \rightarrow SiO_{2(g)}$	$\log P_{SiO_{2(g)}} = \log K + \log P_{O_{2(g)}}$	0.0672 + (16043.28/T)
$Si_{(s)} + O_{2(g)} \rightarrow SiO_{2(s)}$	$\log P_{O_{2(g)}} = -\log K$	9.252 + (47410.44/T)
$Au_{(s)} \rightarrow Au_{(g)}$	$\log P_{Au_{(g)}} = \log K$	6.6484 – (19083.24/T)
$2Au_{(s)} + (3/2)O_{2(g)} \rightarrow Au_2O_3(s)$	$\log P_{O_{2(g)}} = (-2/3)\log K$	13.94 + (88.5/T)

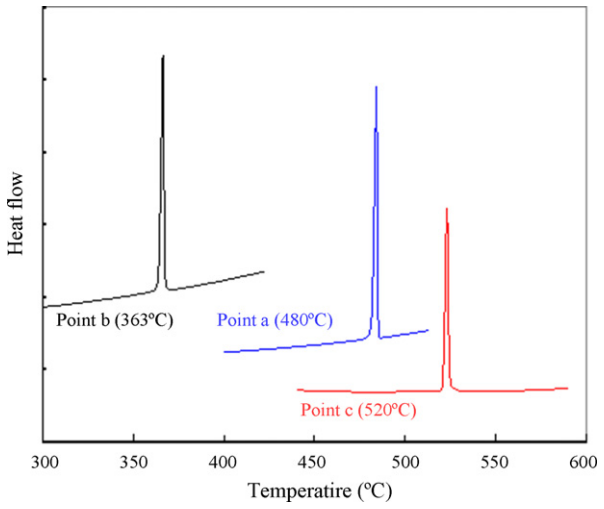

Fig. 4 – DSC thermographs of Au–Si alloys: the melting points of (a) Si–Au (2.3 mass%) at 480 °C, (b) Si–Au (2.8 mass%) at 363 °C, and (c) Si–Au (4.0 mass%) at 520 °C.

deposition, such as a large cost of instruments and a small yield, and the quality of nanowires is jeopardized by the presence of a catalyst required for the ion deposition. In contrast, metal casting is a method well established in metallurgy. The experience gained from this traditional casting combined with emerging nanotechnological methods are prospectively useful in minimizing the cost of nanomaterial fabrication, improving the efficiency of fabrication, and decreasing the complication of the fabrication. For these reasons we fabricated hypoeutectic, eutectic and hypereutectic Au–Si alloys using vacuum smelting; we subsequently formed Au–Si eutectic nanowires by vacuum die-casting using an anodic aluminum-oxide (AAO) thin film as a template.

2. Experiments

Au–Si alloys with three compositions—hypoeutectic (2.3 mass% Si–Au, sample a), eutectic (2.8 mass% Si–Au, sample b), and hypereutectic (4.0 mass% Si–Au, sample c), were fabricated using vacuum smelting. Highly pure (99.99%) gold foil and single-crystal silicon wafers were used for the Au–Si alloys. Samples a–c were placed in quartz tubes that were then evacuated ($P \sim 3 \times 10^{-6}$ Torr) with a turbo molecular pump, purged with argon, and sealed in an oxyacetylene flame. The sealed tubes were heated at 1100 °C for 1 h, with occasional agitation to achieve a homogeneous melt. A schematic diagram is presented in Fig. 2. The melt was then cooled in air to form Au–Si bulk alloys. The metallurgical microstructure and composition of the alloys were examined with an optical microscope (Olympus BX51), a scanning electron microscope

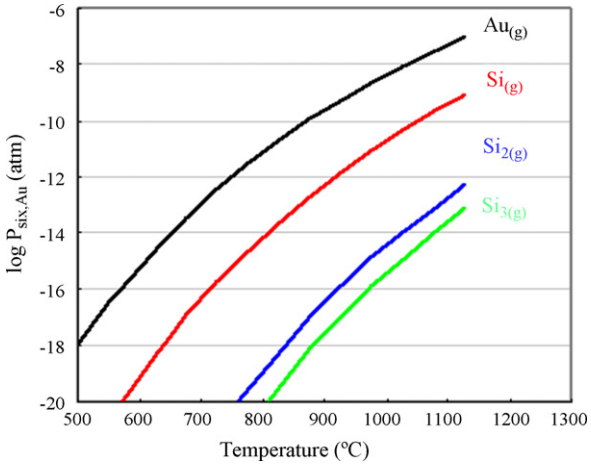

Fig. 5 – Vapor pressures of Au and Si as a function of temperature.

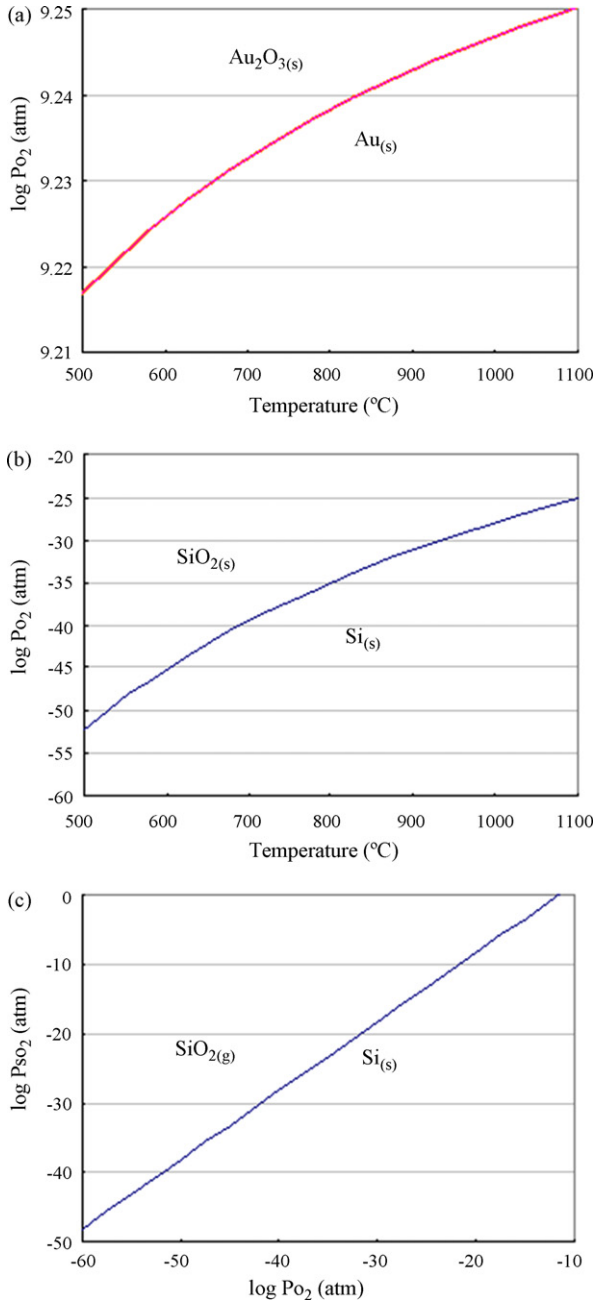

Fig. 6 – Equilibrium partial pressures of oxygen in (a) Au/Au_2O_3, (b) $Si/SiO_{2(s)}$, and (c) $Si/SiO_{2(g)}$.

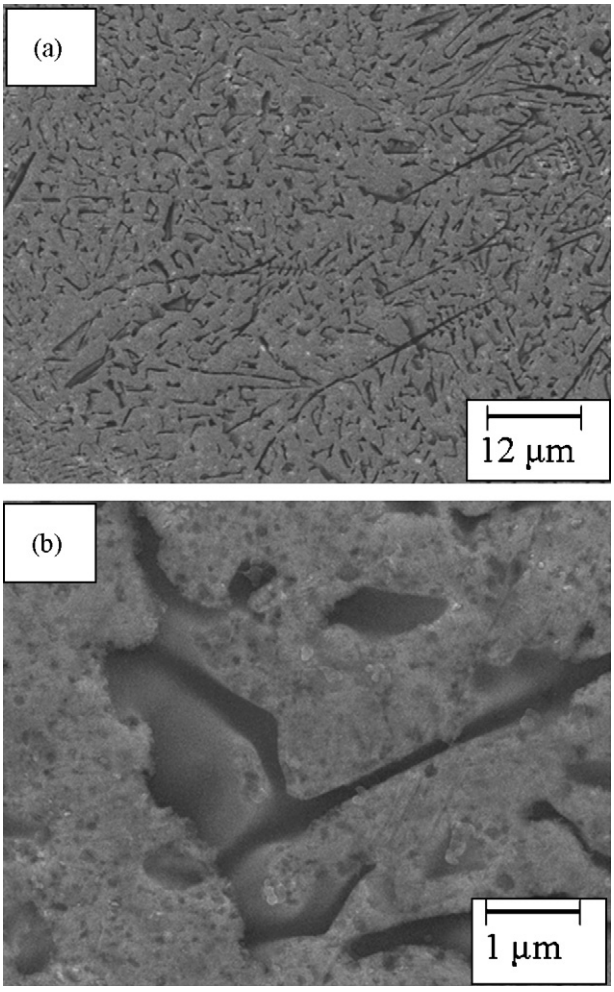

Fig. 7 – SEM images of (a) Au–Si eutectic, (b) zoomed image, and (c) EDS diagram.

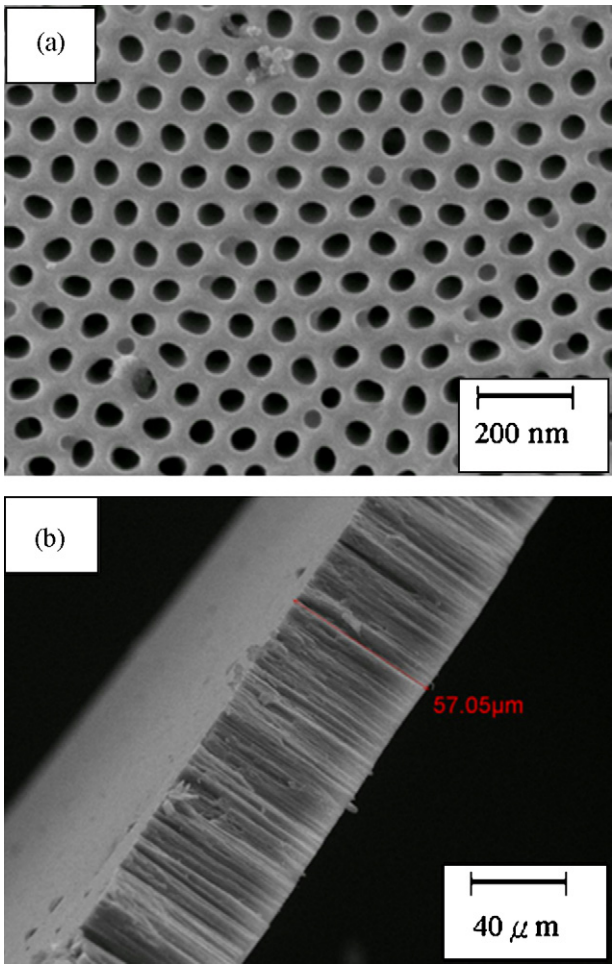

Fig. 8 – SEM images of AAO: (a) top view and (b) side view.

(JEOL 6500F FESEM), X-ray diffraction (Bruker D8), and a differential scanning calorimeter (PerkinElmer Pyris 1). The thermodynamic reaction between Au, Si and O_2 at high temperature was evaluated using thermodynamic data (Chase et al., 1985).

An AAO template (thickness 57 μm) and ordering arrays (pore size 60 nm) were made in oxalic-acid electrolyte (3 mass%); a detailed procedure for AAO fabrication is found elsewhere (Chen et al., 2005; Lin et al., 2006a,b). The Au–Si eutectic nanowires were fabricated using vacuum die-casting (Chen et al., 2006). The morphology of the nanowires was characterized with a SEM, a TEM and an energy dispersive spectrometer (EDX).

3. Results and discussion

Fig. 3 shows OM images of samples a (hypoeutectic), b (eutectic), and c (hypereutectic) after vacuum smelting. The continuous matrix phase is Au, and the discontinuous gray phase is Si. According to the figures, the hypoeutectic has an Au-rich phase (a); the eutectic has homogenous Au and Si mixed phases (b), and the hypereutectic has a Si-rich phase (c). In Fig. 4, DSC curves show the melting points of samples a, b and c – 480, 363 and 520 °C, respectively – matching those shown in Fig. 1. According to the results shown in Figs. 3 and 4, we demonstrated that stoichiometric alloys are obtained according to our experimental conditions.

At high temperatures Au and Si readily form oxides and vaporize: for example, the species $SiO_{2(s)}$, $Si_{(g)}$, $Si_{2(g)}$, $Si_{3(g)}$ and $SiO_{2(g)}$ form in the Si–O system, and $Au_{(g)}$ and $Au_2O_{3(s)}$ form in the Au–O system. The formation of these species causes a loss of composition during alloy smelting; the quantity lost was estimated through a thermodynamic calculation. The reactions of Au, Si, and O_2 are presented in Table 1, in which P denotes partial pressure (atm), T temperature (K), and K equilibrium quotient (Chase et al., 1985). Fig. 5 shows the partial pressures of Au and Si gases as a function of temperature: the partial pressure increases with temperature in an order $Au_{(g)} > Si_{(g)} > Si_{2(g)} > Si_{3(g)}$. Fig. 6 shows the threshold pressure of O_2 of Au and Si for oxidation to $Au_2O_{3(s)}$, $SiO_{2(g)}$ and $SiO_{2(s)}$. The curves show an increasing order $Au_2O_{3(s)} > SiO_{2(g)} > SiO_{2(s)}$, indicating that the formation of $SiO_{2(s)}$ has a smaller threshold of O_2 pressure than formation of $Au_2O_{3(s)}$ and $SiO_{2(g)}$. Hence $Au_{(g)}$ and $SiO_{2(s)}$ are readily lost during Au–Si smelting. Although the pressure of O_2 in the vacuum chamber was small during vacuum smelting, the loss of $Au_{(g)}$ increased with temperature and duration of smelting. As a result, the quantity of

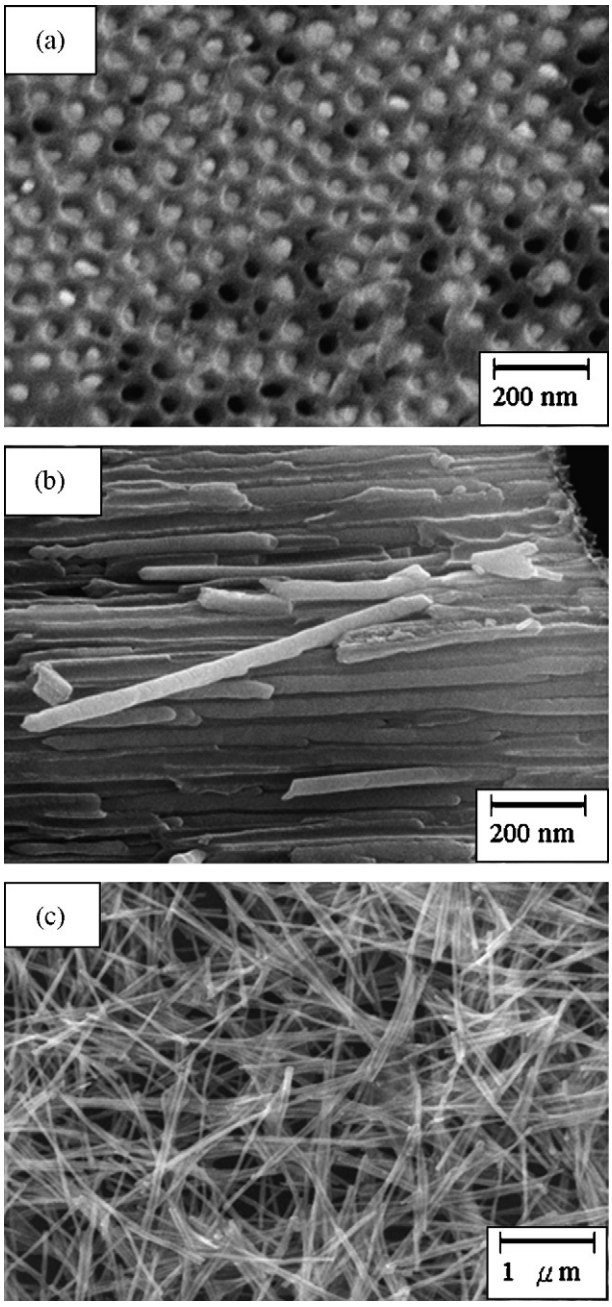

Fig. 9 – SEM images of Au–Si eutectic nanowire in the AAO template: (a) top view, (b) side view, and (c) nanowires removed from the AAO.

Au lost during vacuum smelting is greater than that of Si. In our experiment, the extra Au (0.2 mass%) was added over the eutectic point for Au–Si eutectic formation.

A compound with a ductile matrix and a brittle precipitation structure is typically ductile in bulk. For example, a eutectoid structure of pearlite forms with a ductile Fe matrix and a discontinuous brittle cementite (Fe_3C) precipitation phase (Callister, 1994); a eutectic structure of Sn–Bi alloy forms with a ductile Sn matrix and a discontinuous brittle Bi precipitation phase. The Pb–Bi eutectic is likewise ductile in bulk, but an Au–Si eutectic alloy is a brittle material. Fig. 7 shows SEM

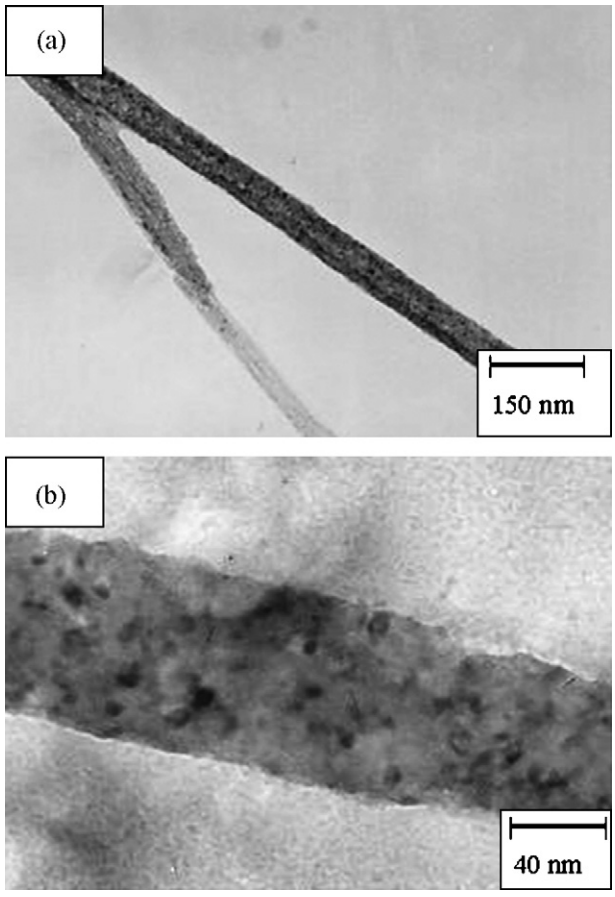

Fig. 10 – TEM images of (a) Au–Si eutectic nanowire and (b) zoomed image of black particle (Si).

images of the Au–Si eutectic microstructure. In the image of Fig. 7(a) at small magnification, a discontinuous phase of Si disperses into the matrix phase of Au. In the image presented in (b) at large magnification, Si is mounted inside Au, and cracks have formed about the Au–Si interface; this cracking makes the Au–Si eutectic brittle. In Au–Si phase diagram, Au and Si cannot form alloy in the Au–Si melt mixture. When the melt mixture was solidified, the solid phases of Au and Si were formed separately. Because the thermal condense coefficients of Au and Si are different (Au: $14.2 \times 10^{-6}\,K^{-1}$, Si: $2.6 \times 10^{-6}\,K^{-1}$) (Dean, 1992), the Au–Si mixture cracks easily, as shown in (b).

Fig. 8 shows SEM images of AAO with ordered nanochannels at the packing density $4 \times 10^{11}\,cm^{-2}$. The pores have diameter 60 nm and length 57 μm. An AAO template of satisfactory quality is required for fabrication of Au–Si nanowires. Fig. 9(a) (top view) and (b) (side view) show SEM images of Au–Si eutectic nanowires produced on vacuum die-casting with an AAO template; (c) shows Au–Si nanowires after the template was dissolved in phosphoric acid (20 vol.%). The diameter and length of the nanowires depend on the AAO size; in this case, the Au–Si eutectic nanowires have diameter ~60 nm and length ~57 μm. To investigate the detailed morphology of individual nanowires that were deposited on a Cu grid after the AAO template was thoroughly dissolved, we employed a TEM: two TEM images of a randomly selected nanowire appear in Fig. 10; the black particles are Si according to EDS.

4. Conclusion

Using vacuum smelting method Au–Si hypoeutectic, eutectic, and hypereutectic alloys were fabricated. Because more Au than Si is lost during this smelting, the extra Au was added to the alloy to achieve an Au–Si eutectic alloy with the correct stoichiometry. The melting points and microstructures of alloys were measured with a differential scanning calorimeter and an optical microscope; these results correlated satisfactorily with the Au–Si phase diagram. Au–Si eutectic nanowires of diameter ~60 nm have been successfully made with die-casting and AAO as a template. SEM and TEM images show the morphology of the nanostructure of Au–Si eutectic nanowires with Si nanoparticles dispersed in the Au matrix.

Acknowledgements

National Science Council of Republic of China (contract 95-2113-M-009-027) and the MOE-ATU program provided financial support.

REFERENCES

Callister Jr, W.D., 1994. Materials Science and Engineering–An Introduction, 3rd ed. Wiley, New York, USA, p. 269.

Chase Jr., M.W., Davies, C.A., Downey Jr., J.R., Frurip, D.J., McDonald, R.A., Syverud, A.N., 1985. JANAF thermochemical tables. J. Phys. Chem. Ref. Data, USA 1650 (1673–1678), 1795–1803.

Chen, C.C., Chen, J.H., Chao, C.G., 2005. Post-treatment method of producing ordered array of anodic aluminum oxide using general purity commercial (99.7%) aluminum. Jpn. J. Appl. Phys. 44, 1529.

Chen, C.C., Bisrat, Y., Luo, Z.P., Schaak, R.E., Chao, C.-G., Lagoudas, D.C., 2006. Fabrication of single-crystal tin nanowires by hydraulic pressure injection. Nanotechnology 17, 367.

Dean, J.A., 1992. Lange's Handbook of Chemistry, 14th ed. McGraw-Hill, New York.

Komatsu, M., Kiritani, M., 2003. Amorphization of eutectic alloys by shock compression. Mater. Sci. Eng. A 350, 150.

Lin, J.S., Chen, Y.C., Chen, C.-C., Diau, E.W.-G., Liu, T.-F., 2006a. Aggregation of zinc protoporphyrin in anodized aluminum oxide (AAO) nanoporous environments. J. Chin. Chem. Soc. 53, 201.

Lin, J.S., Chen, Y.C., Chen, C.-C., Luo, L.-Y., Diau, E.W.-G., Liu, T.-F., 2006b. Fluorescence dynamics of zinc protoporphyrin in solution and inside anodized aluminum oxide (AAO) nano-channel arrays. J. Chin. Chem. Soc. 53, 1405.

Massalski, T.B., 1987. Binary alloy phase diagrams. Am. Soc. Met., USA, 313.

Nielsch, K., Wehrspohn, R.B., Barthel, J., Kirschner, J., Gosele, U., Fischer, S.F., Kronmuller, H., 2001. Hexagonally ordered 100-nm period nickel nanowire arrays. Appl. Phys. Lett. 79, 1360.

Wan, Q., Wang, T.H., Lin, C.L., 2004. Self-assembled Au–Si alloy nanocones: synthesis and electron field emission characteristics. Appl. Surf. Sci. 221, 38.

Wang, B., Yin, S., Wang, G., Buldum, A., Zhao, J., 2001. Novel structures and properties of gold nanowires. Phys. Rev. Lett. 86, 2046.

Zhang, Y.F., Tang, Y.H., Wang, N., Lee, C.S., Bello, I., Lee, T., 2000. Germanium nanowires sheathed with an oxide layer. Phys. Rev. B 61, 4518–4521.

Zhirnov, V.V., Bormatova, L., Givargizov, E.I., 1996. Field emission properties of Au–Si eutectic. Appl. Surf. Sci. 94/95, 144.